Chemical Science

Accepted Manuscript

This article can be cited before page numbers have been issued, to do this please use: M. Agrachev, W. Fei, S. Antonello, S. Bonacchi, T. Dainese, A. Zoleo, M. Ruzzi and F. MARAN, *Chem. Sci.*, 2020, DOI: 10.1039/D0SC00520G.




ROYAL SOCIETY OF CHEMISTRY

rsc.li/chemical-science

ROYAL SOCIETY OF CHEMISTRY View Article Online
DOI: 10.1039/D0SC00520G

Journal Name

ARTICLE



# Understanding and Controlling the Efficiency of $Au_{24}M(SR)_{18}$ Nanoclusters as Singlet-Oxygen Photosensitizers†

Received 00th January 20xx,
Accepted 00th January 20xx

DOI: 10.1039/x0xx00000x

www.rsc.org/

Mikhail Agrachev,[a,b] Wenwen Fei,[a,b] Sabrina Antonello,[a] Sara Bonacchi,[a] Tiziano Dainese,[a] Alfonso Zoleo,[a] Marco Ruzzi,*[,a] and Flavio Maran*[,a,b]

Singlet oxygen, $^1O_2$, can be generated by molecules that upon photoexcitation enable the $^3O_2 \rightarrow {}^1O_2$ transition. We used a series of atomically precise $Au_{24}M(SR)_{18}$ clusters, with different R groups and doping metal atoms M. Upon nanosecond photoexcitation of the cluster, $^1O_2$ was efficiently generated. Detection was carried out by time-resolved electron paramagnetic resonance (TREPR). The resulting TREPR transient yielded the $^1O_2$ lifetime as a function of the nature of the cluster. We found that: these clusters indeed generate $^1O_2$ by forming a triplet state; a more positive oxidation potential of the molecular cluster corresponds to a longer $^1O_2$ lifetime; proper design of the cluster yields results analogous to those of a well-known reference photosensitizer, although more effectively. Comprehensive kinetic analysis provided important insights into the mechanism and driving-force dependence of the quenching of $^1O_2$ by gold nanoclusters. Understanding on a molecular basis why these molecules may perform so well in $^1O_2$ photosensitization is instrumental to control their performance.

## Introduction

Singlet oxygen, $^1O_2$, is the first excited state ($^1\Delta_g$) of molecular oxygen. Depending on the experimental conditions, its lifetime can span orders of magnitude.[1-3] $^1O_2$ eventually converts to ground-state triplet oxygen ($^3\Sigma_g^-$), $^3O_2$. Because singlet oxygen is significantly more reactive than triplet oxygen, it finds uses in several applications, especially organic synthesis, photocatalysis, and nanomedicine (photodynamic therapy).[4-9] Singlet oxygen[10-12] can be produced by direct excitation, although the $^3O_2 \rightarrow {}^1O_2$ is a spin-forbidden transition with a very low absorption coefficient. A more efficient way to generate singlet oxygen is by using photosensitizers.[10,13] The sensitizer is photoexcited to its singlet state, undergoes intersystem crossing (ISC) to form the excited triplet state, and then transfers energy to triplet oxygen to yield $^1O_2$; the last step is efficient because the overall angular moment is now conserved. Suitable photosensitizers are molecules that exhibit a sufficiently high value of the excited triplet-state energy (the $^3\Sigma_g^-$ to $^1\Delta_g$ excitation energy, $E_{exc}$, is 94 kJ mol$^{-1}$), a high quantum yield for ISC, and a sufficiently long triplet lifetime. On the other hand, it has been long acknowledged that the sensitizer and/or products of its photoreactions can also quench singlet oxygen by converting it back to $^3O_2$.[14,15] These quenching reactions may significantly diminish the $^1O_2$ lifetime and, consequently, affect the overall efficiency of the photosensitization process. An ideal photosensitizer should, therefore, maximize generation efficiency and minimize deactivation. This is not, however, an easy task to achieve.[10]

The detection of singlet oxygen in fluid solution is routinely carried out with optical spectroscopies. The most specific probe of singlet oxygen is the 1275 nm $^1O_2 \rightarrow {}^3O_2$ phosphorescence, particularly when it is monitored in a time-resolved experiment. To overcome the low-sensitivity limitations, several approaches have been proposed, mostly relying on the introduction of a fluorescent probe activated by energy transfer from $^1O_2$. For example, phthalocyanines, naphthalocyanines, and porphyrazines exhibit strong delayed luminescence upon energy transfer from two $^1O_2$ molecules.[16] This luminescence is emitted in the visible-light region and its quantum yield exceeds that of $^1O_2$ phosphorescence by 2-4 orders of magnitude. These molecules, however, are also good sensitizers for the formation of $^1O_2$, thereby complicating detection. Chemical traps have also been extensively employed.[17] Singlet oxygen rapidly and irreversibly reacts with aromatic compounds to yield endoperoxides that do not fluoresce and whose absorption spectrum differs significantly from that of the original molecule. However, chemical traps may also be reactive toward other reactive oxygen species. Because of the difficulties associated with direct detection and indirect methods, alternative approaches for the detection of $^1O_2$ generated by photosensitizers are thus sought.

Possible photosensitizer candidates that meet several of the aforementioned requirements are atomically precise gold

[a] Department of Chemistry, University of Padova, Via Marzolo 1, 35131 Padova, Italy.
[b] Co-first authors.
[c] Department of Chemistry, University of Connecticut, 55 North Eagleville Road, Storrs, 06269 Connecticut, USA.

† Electronic Supplementary Information (ESI) available: Chemicals, determination of relevant kinetic and thermodynamic parameters, further experimental procedures, Table S1, Figures S1–S9. See DOI: .....

nanoclusters, $Au_n(SR)_m$ (where SR = thiolate). Nowadays, many of these clusters can be prepared in a very pure, controlled state.[18] This implies full molecular control on structure and properties, which cannot be achieved with the larger gold nanoparticles. Because the electronic structure and thus the optical properties of these clusters depend on the values of n and m, ultrasmall gold nanoclusters might be, in principle, optimized for efficient production of $^1O_2$. So far, the research in this field has been quite limited,[19-33] with very few examples describing the behavior of truly atomically precise gold nanoclusters. This is the case of $Au_{25}(SR)_{18}$, which is a stable cluster that shows distinct electrochemical,[34] optical,[18] and magnetic features,[35,36] and is consistently considered the benchmark system for understanding and controlling many properties of gold nanoclusters.[37,38] Kawasaki *et al.* were the first to describe the formation of singlet oxygen using $Au_{25}(SR)_{18}$ (HSR = phenylethanethiol or captopril) as photosensitizer.[19] The photosensitization was detected optically and with chemical quenchers. $Au_{38}(SC_2H_4Ph)_{24}^0$, another well-established molecular cluster, was found to be significantly less efficient. More recently, Ho-Wu et al. compared the photosensitization efficiency of $Au_{25}$, $Ag_{32}$, $Au_{144}$, larger gold nanoparticles, and a conventional dye photosensitizer.[29] This study, which was carried out with indirect optical methods (1,3-diphenylisobenzofuran quencher), concluded that $Au_{144}$ provides the most efficient system. A size dependence order of $Au_{144}$ > $Au_{38}$ > $Au_{25}$ was observed for the aerobic oxidation of D-Glucose on carbon-supported clusters.[31] The efficiency of $^1O_2$ generation using $Au_{38}S_2(SAdm)_{20}$ (SAdm = adamantanethiolate) nanoclusters was found to be higher than that of $Au_{25}(SC_2H_4Ph)_{18}^-$.[32] The ultrasonic activation of $Au_{25}(Captopril)_{18}$ to generate $^1O_2$ was also demonstrated.[33]

Here we describe the photosensitizing behavior of a series of $Au_{25}(SR)_{18}^-$, where R = *n*-$C_3H_7$ (C3), *n*-$C_4H_9$ (C4), and $C_2H_4Ph$ (C2Ph) (hereafter, we will indicate the number of carbon atoms of the alkyl chain simply as Cn), and monodoped $Au_{24}M(SR)_{18}$ (M = Cd, Hg) clusters (Figure 1). Besides studying the effect of the protecting ligand, the analysis was extended to monodoped clusters because their optical and especially electrochemical behaviors show significant differences from those of the undoped clusters.[39] Regarding detection, we relied on continuous-wave and, especially, time-resolved electron paramagnetic resonance techniques (CWEPR and TREPR, respectively). TREPR spectroscopy provides an efficient and sensitive method to detect even very low concentrations of $^1O_2$ generated by photosensitization in solution.[40,41] Moreover, TREPR is selective toward singlet oxygen, which is unequivocally detected and identified, while other reactive oxygen species are not revealed. As we will show, TREPR allowed us to characterize in detail the photosensitization behavior of the investigated clusters, and could confirm that the cluster's excited state responsible for the generation of singlet oxygen is indeed a triplet. Most notably, we found that proper design of the redox properties of the cluster yields results comparable to those of tetraphenylporphirin (TPP), which is a well-known reference photosensitizer.[10] Finally, we carried out a comprehensive kinetic investigation on the $^1O_2$ quenching mechanism by gold nanoclusters as a function of driving force and obtained important mechanistic insights into the reasons why properly devised gold nanoclusters may perform very well in $^1O_2$ photosensitization.

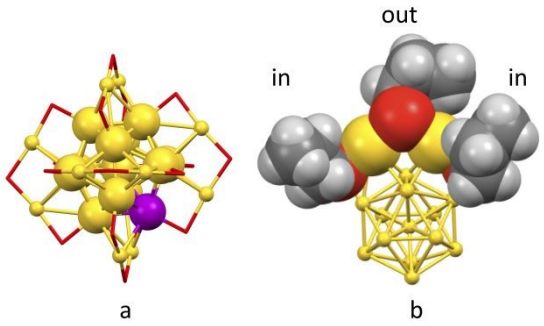


**Figure 1.** (a) Typical structure of the $Au_{24}M(SR)_{18}$ nanocluster. One of the icosahedron positions (pink) corresponds to M (M = Au, Hg, Cd). The gold (yellow) and sulfur (red) atoms are shown, whereas the carbonaceous part of the ligands is omitted for clarity. (a) Structure of $Au_{25}(SC3)_{18}^0$ showing the C (gray) and H atoms (white) for both inner (in) and outer (out) ligand types of one of the six staples.

## Results and Discussion

### $^1O_2$ Photosensitization with TREPR Detection

TREPR spectroscopy is especially suitable to study the kinetics of photogenerated paramagnetic species exhibiting lifetimes ranging from few to several hundred μs.[42] TREPR detection of $^1O_2$ is based on the radical triplet pair (RTP) mechanism.[43] Triplet quenching by a stable free radical, such as a nitroxide (which is a doublet, $^2R$, and generally exhibits three, very similar CWEPR signals due to the hyperfine interaction of the unpaired electron with the N nucleus), induces populations of the radical spin sublevels that differ significantly from those at thermal equilibrium. This phenomenon, which is commonly referred to as chemically induced dynamic electron polarization,[44] can be sensitively detected by TREPR in the form of transient intensities of the EPR signals associated with the radical probe. Importantly, polarization may be also caused by a singlet state, as in the case of $^1O_2$.[45,46]

Briefly, photoexcitation of the sensitizer fundamental singlet state ($^1PS$) yields a singlet excited state ($^1PS^*$) that is quickly converted into a triplet state ($^3PS^*$) via ISC. In the absence of oxygen, the excited triplet state undergoes quenching by interaction with a nitroxide radical, and *polarized emissive* TREPR signals are observed. The emissive polarization is interpreted according to the quartet-precursor RTP (Q-RTP) theory,[47] as described by eq 1:

(1) $^3PS^* + {}^2R \longrightarrow {}^1PS + {}^2R^*\downarrow$

where $^2R^*\downarrow$ indicates the emissive spin polarization generated in $^2R$ by the quenching of the $^3PS^*$ state. Radicals, on the other hand, are also able to quench singlet states, though now the spin polarization is opposite to that just described: in an air-saturated solution of a nitroxide and a triplet sensitizer, a



 

*reinforced absorptive polarization* for the signals of the nitroxide is indeed expected. This absorptive character of the polarization is a consequence of the initial energy exchange of the triplet state of the sensitizer by triplet oxygen to form $^1O_2$ (eq 2), which then polarizes the radical $^2R$ (eq 3):

(2) $^3PS^* + {}^3O_2 \longrightarrow {}^1PS + {}^1O_2$

(3) $^1O_2 + {}^2R \longrightarrow {}^3O_2 + {}^2R^*\uparrow$

where $^2R^*\uparrow$ refers to the radical in which reinforced absorptive spin polarization is generated. This mechanism is the equivalent of the doublet-precursor RTP (D-RTP) theory,[45] the only difference being that now the nitroxide interacts with a singlet, rather than a triplet state. Very important, the magnitude of this net absorptive spin polarization is *extraordinarily large* even for traces of singlet oxygen.[46]

All clusters were prepared and characterized by mass spectrometry, NMR spectroscopy, and UV-vis spectroscopy as described previously.[39,48-50] Special care was paid on controlling properly the charge state.[51,52] TREPR experiments were carried out in toluene at 240 K, and refer to 1 mM cluster and 0.5 mM 2,2,6,6-tetramethyl-4-oxo-1-piperidinyloxy (TEMPONE), unless otherwise stated. In TREPR, a laser pulse (we used 4 ns at 532 nm) triggers the aforementioned photochemical reaction/s and eventually generates the polarized paramagnetic species ($^2R^*\uparrow$ or $^2R^*\downarrow$). The ensuing EPR transient is recorded at the given value of the magnetic field (*B*). This procedure is applied by scanning *B* until the entire field range is covered. The sequence is then repeated many times, and the corresponding series of transients is averaged. The resulting TREPR spectrum is usually displayed in a 3D form (Figure 2), where the TREPR intensity is plotted as a function of *B* and time (*t*). No field modulation is applied and thus the observed signals do not exhibit the derivative shape typical of the corresponding CWEPR spectra (Figure 3c,d).

Figure 2a shows the spectrum obtained using $Au_{25}(SC3)_{18}^-$ as the photosensitizer under aerobic conditions. The TREPR spectrum of TEMPONE consists in three signals of equal intensity that decay in a few µs. The polarized TREPR signals show the net absorptive character expected when the overall photosensitization process (excitation, ISC, and energy transfer) is efficient and followed by step (3). In the control experiment carried out in the absence of oxygen, only emissive polarization is observed (Figure 2b). According to the Q-RTP mechanism, the emissive polarized transient spectra are consistent with the direct interaction of the nitroxide with the triplet state of $Au_{25}(SR)_{18}^-$. The extent of emissive polarization strongly depends on the quantum yield of the latter and the actual lifetime of the cluster triplet state. In this connection, the different time scales of the transients in the two plots of Figure 2 are worth noticing. These results already allow us to draw a very important conclusion. So far, photoexcitation of clusters has been generically described as generating excited states, as no conclusive evidence about the formation of an excited triplet state could be gathered. In the first report on singlet oxygen generation by photoexcited Au clusters, the term triplet state was used for the very same reason that the photoexcited cluster was generating $^1O_2$.[19] On the other hand, singlet oxygen may form in several different ways.[53] In the present context, the TREPR results observed under anaerobic conditions definitely prove that, indeed, photoexcitation of $Au_{25}(SR)_{18}^-$ eventually leads to an excited triplet state.[46]

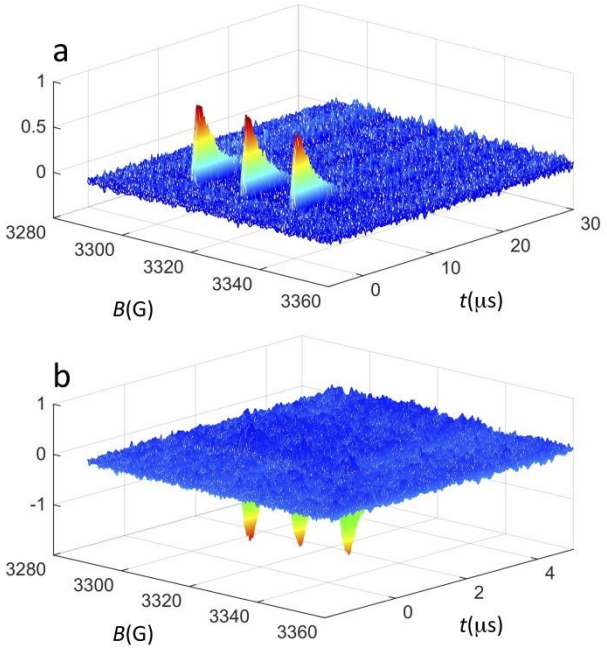


**Figure 2.** TREPR surfaces recorded for 0.5 mM TEMPONE and 1 mM $Au_{25}(SC3)_{18}^-$ in (a) air-saturated and (b) deaerated toluene solution at 240 K. The z-axis shows the TREPR intensity (a.u.).

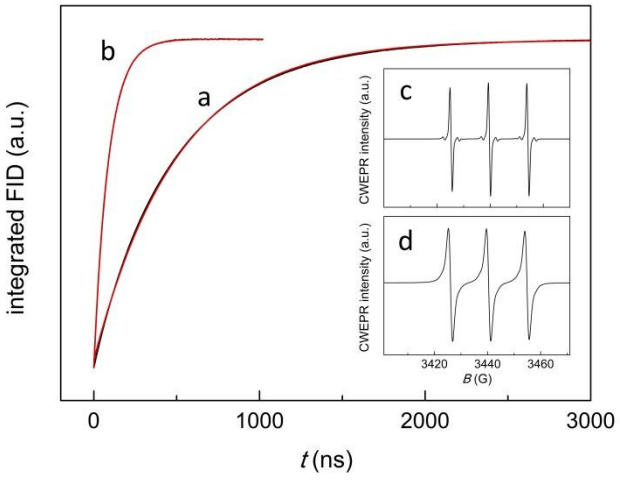


**Figure 3.** Inversion recovery curves for a toluene solution of 0.5 mM TEMPONE and 1 mM $Au_{25}(SC3)_{18}^-$ (black) under anaerobic (trace a) and aerobic conditions (trace b), with the corresponding exponential fits to the data (red: for both curves, $r^2 = 1.000$). The CWEPR spectra refer to the corresponding anaerobic (c) and aerobic conditions (d).

### Analysis of the $^1O_2$ Lifetime and Validation of the TREPR Method

The decay kinetics depends on several parameters. In a deaerated solution, the decay of the emission-polarized signals

View Article Online DOI: 10.1039/D0SC00580G





(Figure 2b) is determined by the lifetime of the cluster triplet state and the characteristic magnetic-relaxation times of the nitroxide, T1 and T2.[54] T1, which is the spin-lattice longitudinal relaxation time, can be determined independently, by pulsed EPR inversion recovery experiments (Figure 3, trace a), to be 499.1(0.6) ns. In the absence of the cluster, we obtained the virtually identical value of 501.8(0.7) ns ($r^2$ = 1.000). T2 is the transverse spin-spin relaxation time, and could be estimated to be 0.43(0.01) µs from the reciprocal of the full-width-at-half-height of the integral of the CWEPR spectrum shown in Figure 3c, as illustrated in Figure S1. In deaerated solution, the reciprocal of the TREPR decay rate-constant value obtained from the emission data (Figure S2) is 0.45(0.01) µs ($r^2$ = 0.983), and therefore, is comparable to the relaxation parameters of TEMPONE. These results point to the TEMPONE spin relaxation as a particularly relevant factor determining the TREPR decay kinetics, and thus imply that the lifetime of the cluster triplet state should be shorter than ~0.3 µs.

In the presence of air, the CWEPR spectrum of TEMPONE shows broader peaks (Figure 3d). The T1 measured by pulsed EPR inversion recovery experiments in the presence of $Au_{25}(SC3)_{18}^-$ (Figure 3b) is now only 64(0.2) ns ($r^2$ = 1.000), that is, about one order of magnitude shorter than the T1 determined under anaerobic conditions. Similarly, T2 decreases from 0.43 to 0.04 µs. These effects are caused by the known interaction of TEMPONE with triplet oxygen.[55] Under aerobic conditions, the decay of the TREPR signals also depends on the singlet-oxygen lifetime. A scheme of the general process is provided in the inset of Figure 4. The average of the TREPR transients (Figure 4) can be fit to single

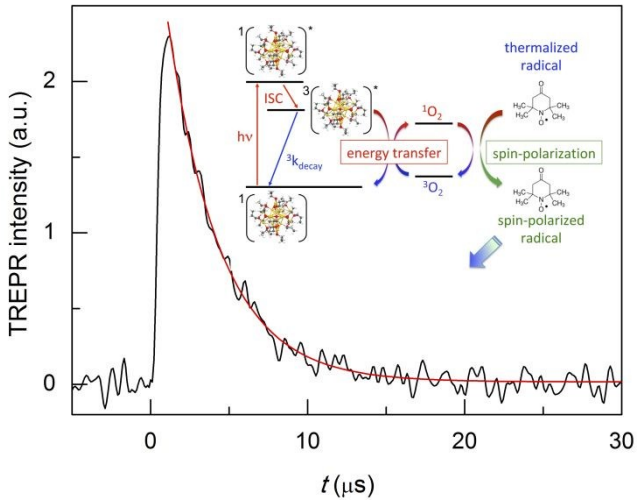


**Figure 4.** TREPR transient observed for 0.5 mM TEMPONE and 1 mM $Au_{25}(SC3)_{18}^-$ in toluene under aerobic conditions (black) at 240 K. The red curve is the exponential fit to the data. The inset provides a schematic representation of the TREPR detection of $^1O_2$ generation through photoexcitation of the cluster.

exponential ($r^2$ = 0.969) yielding an observed decay rate constant ($k_\Delta$) of 3.02 x $10^5$ $s^{-1}$, which corresponds to a lifetime ($\tau_\Delta$) of 3.31(0.05) µs. $\tau_\Delta$ is thus nearly two orders of magnitude longer than the corresponding T1 value, and this indicates that now the observed decay of spin polarization is only controlled by the $^1O_2$ lifetime. In other words, while the polarized signals decay on the T1 time scale, there is still some singlet oxygen in solution that continuously contributes to generate further polarization in the TEMPONE molecules. Under these conditions, the decay of the TREPR signal lifetime can thus be used to calculate the singlet-oxygen lifetime.

In any given experimental condition, the observed $^1O_2$ lifetime is determined by the species present in solution.[10] In the absence of solutes other than oxygen, on the other hand, the intrinsic $^1O_2$ decay pseudo-first order rate constant ($k_\Delta^S$) only depends on the solvent (S) through two terms (eq 4):

$$(4)\quad k_\Delta^S = k_{nr}[S] + k_r[S]$$

where $k_{nr}$ and $k_r$ refer to the nonradiative and radiative components, respectively.[10,56] From available data obtained in toluene as a function of temperature, we calculate for the intrinsic lifetime of $^1O_2$ ($\tau_\Delta^S$) at 240 K the values of 31.7[57] and 34.6 µs.[56] These lifetimes are significantly longer than the value of 3.31 µs obtained with the TEMPONE/$Au_{25}(SC3)_{18}^-$ system, and therefore, show that in our experimental conditions significant quenching of singlet oxygen must take place. Comparison of $\tau_\Delta$ with $\tau_\Delta^S$ (hereafter, we will refer to the most recent determination, 34.6 µs)[56] yields a relative $\tau_\Delta$ decrease of 100($\tau_\Delta^S$ - $\tau_\Delta$)/$\tau_\Delta^S$ = 90.4%.

Besides the solvent, there are two possible candidates as quenchers: TEMPONE and the cluster itself. To address this issue, we carried out further experiments. The majority of photosensitizers currently employed in photodynamic therapy are cyclic tetrapyrrolic structures, such as porphyrin derivatives.[58] It is thus instructive to compare the polarized signals observed for $Au_{25}(SC3)_{18}^-$ with those obtained for tetraphenylporphyrin (TPP), which is a well-known reference photosensitizer, yet showing some quenching of $^1O_2$.[59] TPP was used at the same concentration of the cluster (1 mM) and qualitatively gave the same TREPR spectrum, but for the two differences that the signal intensity at its maximum is ~3 times larger than for $Au_{25}(SC3)_{18}^-$ and, particularly important, the decay is much slower (Figure 5). It should be noted that for $t$ < 0.5 µs the presence of a negative spike indicates that a (small) fraction of the amount of the TPP molecules in their triplet excited state (for TPP, the fraction of singlet excited state species that undergo radiationless decay to form the triplet excited state is $\Phi_T$ = 0.71;[60] in the presence of oxygen, this value is expected to increase slightly)[61] reacts with TEMPONE according to the Q-RTP theory (eq 1). The fact that the TREPR intensity maximum is attained in 1.5-2 µs, indicates that the majority of the TPP triplet reacts with $^3O_2$ within less than 1 µs. This is in keeping with a lifetime of 196 ns measured for the TPP triplet state in aerated toluene at room temperature.[62]

Best fit of the decay data obtained for $t$ > 3 µs gives $k_\Delta$ = 3.54 × $10^4$ $s^{-1}$ ($r^2$ = 0.999), corresponding to a lifetime $\tau_\Delta$ of 28.2(0.1) µs. This shows that TPP is, as expected, a very good photosensitizer. Comparison of this $\tau_\Delta$ value with $\tau_\Delta^S$, however, evidences a relative $\tau$ decrease of 18.5%. To obtain information on a possible effect of TEMPONE as a quencher, we carried out further TPP photosensitization experiments in which the TEMPONE concentration was varied, as exemplified

 

View Article Online
DOI: 10.1039/D0SC00530G



by the two traces in Figure 5. We obtained: [TEMPONE] = 0.2 mM, $k_\Delta$ = 3.36 × $10^4$ $s^{-1}$, $\tau_\Delta$ = 29.8(0.4); ([TEMPONE] = 0.1 mM, $k_\Delta$ = 3.66 × $10^4$ $s^{-1}$, $\tau_\Delta$ = 27.4 (0.6). The very similar $\tau_\Delta$ values, therefore, show that under our experimental conditions the TEMPONE concentration does not affect the observed $^1O_2$ lifetime. Besides confirming that indeed TPP acts as a quencher, these results also indicate that despite the intense TREPR signals, TEMPONE polarization must involve a very small amount of the $^1O_2$ present in solution. These tests validated the TREPR methodology and indicated that 0.5 mM TEMPONE could be consistently used with no detectable effect on the $^1O_2$ lifetime. The experiments described below were carried out under these conditions.

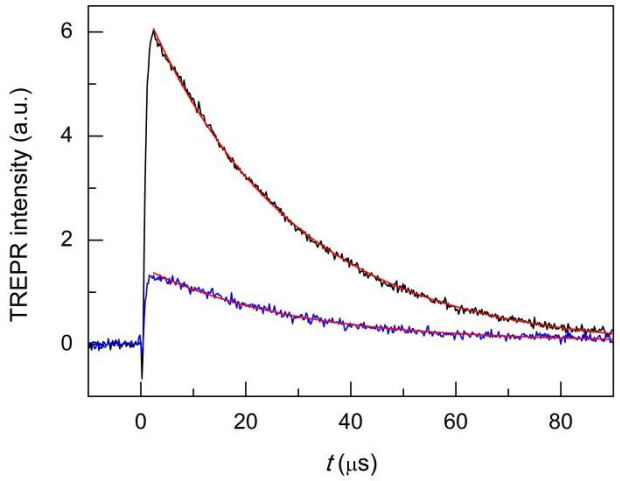


**Figure 5.** TREPR transients observed under aerobic conditions for samples of 1 mM TPP and 0.5 (black) or 0.1 mM (blue) TEMPONE in toluene at 240 K. The corresponding exponential fits to the data are in red.

**Tuning the Photosensitizing Properties of $Au_{25}$ Nanoclusters**

The TREPR data confirm that $Au_{25}(SR)_{18}^-$ can be used as a photosensitizer.[19] They also show that the $^1O_2$ lifetime measured in the presence of $Au_{25}(SC3)_{18}^-$ is much shorter than the $\tau_\Delta^S$ value. The cluster is, therefore, a good sensitizer but also a good quencher, as observed for many sensitizers.[10] We will now specifically focus on this aspect. The decay of singlet oxygen can proceed by physical quenching, leading to deactivation of $^1O_2$, and chemical reactions, in which $^1O_2$ irreversibly reacts with some other species in solution.[10] In the presence of a generic molecule (M) capable of quenching or chemically reacting with $^1O_2$, eq 4 must include further terms (eq 5):[10,56]

(5) $k_\Delta = k_{nr}[S] + k_r[S] + k_q[M] + k_{cr}[M]$

where $k_q$ and $k_{cr}$ are the second-order rate constants referring to the quenching and chemical reaction components, respectively. The gold nanoclusters do not react chemically with $^1O_2$. Although $Au_{25}(SR)_{18}^-$ may react with $^1O_2$ by electron transfer (ET), the effect of this reaction is detected only on a much longer time scale. For example, we found that flashing a $Au_{25}(SC4)_{18}^-$ sample (by using the same pulse sequence as in the TREPR experiments) in the presence of oxygen for 2 h transforms 8.8% of the anion into the corresponding neutral cluster (Figure S3). We can now thus focus only on the physical quenching paths, which consist in the first three terms in eq 5. Physical quenching is the consequence of interactions with the solvent (terms $k_{nr}$ and $k_r$) and solute/s (term $k_q$). For many solvents, including toluene, $k_{nr}$ is dominant over $k_r$.[10] As to $k_{nr}$, solvent molecules deactivate singlet oxygen by electronic-vibrational energy transfer and by perturbing singlet oxygen with the result of facilitating its transition to $^3O_2$.[12,56] An effective physical quenching route is also attributed to the formation of a charge-transfer (CT) complex between singlet oxygen and the photosensitizer.[10,63,64] The resulting exciplex is a bimolecular excited state that can be described as a resonance of the excited and full ET states. The exciplex thus involves a partial (δ) CT[10] and its formation favors ISC[64-67] by providing a spin-orbit coupling contribution that helps overcoming the spin constrain associated with the $^1O_2 \rightarrow {}^3O_2$ transition.[68] Exciplex formation is especially favored when the photosensitizer is a good electron-donating compound.[10] This is a condition that applies particularly well to $Au_{25}(SR)_{18}^-$ clusters, whose formal potential ($E°$) values ($Au_{25}(SR)_{18}^0/Au_{25}(SR)_{18}^-$ redox couple) are, compared with usual photosensitizers,[10] exceptionally low. In dichloromethane (DCM) containing 0.1 M tetrabutylammonium hexafluorophosphate (TBAH), which is the solvent/electrolyte system generally used to study and compare the electrochemical behavior of metal nanoclusters,[34] the $E°$ of, *e.g.*, the $Au_{25}(SC3)_{18}^0/Au_{25}(SC3)_{18}^-$ redox couple is -0.171 V (298 K, potentials versus the saturated calomel electrode, SCE),[49] whereas that of the $O_2/O_2^{-\bullet}$ is -0.85 V (this work).

The easiest way to tune the properties of $Au_{25}$ is to change the capping ligands. Whereas this change does not affect the structure and the absorption spectrum,[18,69] other properties, especially the electrochemical potentials,[34,70] may change appreciably. Finally, the ligands provide a nanoenvironment surrounding the cluster core that determines the effective dielectric constant[70] and porosity of the capping monolayer,[69] and these factors may exert an influence on the quenching mechanisms of the excited states and ultimately the effective singlet-oxygen lifetime. To gain insights into this aspect, we compared the outcome of TREPR measurements carried out on $Au_{25}$ clusters capped by SC3, SC4, and SC2Ph thiolates. The ligand choice was primarily dictated by their ability to change the $E°$ of the $Au_{25}(SR)_{18}^0/Au_{25}(SR)_{18}^-$ redox couples quite significantly.[70,71]

$Au_{25}(SC4)_{18}^-$ and $Au_{25}(SC2Ph)_{18}^-$ display TREPR surfaces similar to $Au_{25}(SC3)_{18}^-$. Figure 6 compares the reinforced absorptive-polarized transient signals observed upon $^1O_2$ photosensitization by $Au_{25}(SC4)_{18}^-$, $Au_{25}(SC3)_{18}^-$, and $Au_{25}(SC2Ph)_{18}^-$ (red, black, and blue traces, respectively). The growth of the polarized signals occurs within 1 μs (that is, a bit faster than for TPP) and the maximum signal intensities are very similar, pointing to similar photosensitization efficiency (in Figure 6 the intensities are normalized for the sake of better comparison of the transients).

View Article Online
DOI: 10.1039/D0SC00530G

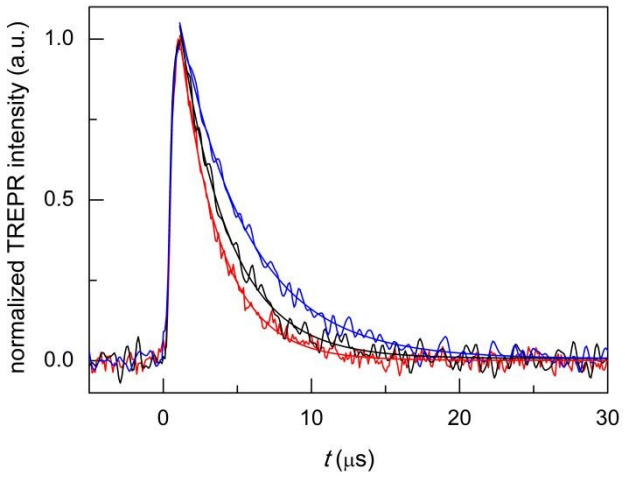


**Figure 6.** TREPR (normalized) transients and corresponding exponential fits to the data for air-saturated toluene solutions of 0.5 mM TEMPONE and 1 mM $Au_{25}(SC4)_{18}^-$ (red), $Au_{25}(SC3)_{18}^-$ (black), and $Au_{25}(SC2Ph)_{18}^-$ (blue). Temperature = 240 K.

Monoexponential fit to the decay data reveals small, yet clearly detectable differences in the value of $k_\Delta$, which increases in the order $Au_{25}(SC2Ph)_{18}^-$ ($2.17 \times 10^5$ $s^{-1}$, $r^2 = 0.990$) < $Au_{25}(SC3)_{18}^-$ ($3.02 \times 10^5$ $s^{-1}$, $r^2 = 0.974$) < $Au_{25}(SC4)_{18}^-$ ($3.69 \times 10^5$ $s^{-1}$, $r^2 = 0.986$); the corresponding lifetimes $\tau_\Delta$ are 4.61(0.05), 3.31(0.05), and 2.71(0.04) μs, respectively. This order indeed matches that of the decreasing $E°$s of the anionic clusters (DCM/0.1 M TBAH, 298 K, $E$ vs SCE), which are -0.077, -0.171, and -0.188 V, respectively.[70,71] These data point to the ease of oxidation (lower $E°$ value) as an important factor enhancing the cluster quenching ability, and are thus in keeping with the effect noted for other sensitizer families.[10]

Overall, these results evidence a detectable effect of the cluster oxidation potential on the singlet-oxygen decay kinetics, and thus confirm an active role of the cluster also as a quencher. With alkanethiolate ligands, however, the potentials cannot be changed substantially.[34,70] A more substantial way to modify the physicochemical properties of gold nanoclusters is by doping their core with other metals. We thus focused on modifying $Au_{25}(SC4)_{18}^-$ to prepare the corresponding $Au_{24}M(SC4)_{18}^0$ clusters, with M = Hg, Cd. For these metals, monodoping is conveniently accomplished by carrying out the metal exchange on a preformed $Au_{25}(SR)_{18}^-$ cluster by using a salt or thiolate of the exogenous metal.[39,72-74] We focused on these two metals because they both dope the cluster on one of the icosahedron positions, as we could demonstrate very recently.[39] While in their neutral state, the resulting $Au_{24}M(SC4)_{18}^0$ clusters are diamagnetic and thus match the same magnetic state of anion $Au_{25}(SC4)_{18}^-$.

Monodoping affects the HOMO-LUMO gap. The values that can be estimated from the electrochemical peaks are:[39,70] Au, 1.30 eV; Hg, 1.28 eV; Cd, 1.41 eV. Similar differences are found for the optical bandgaps.[39,75] These differences are indeed noteworthy because, for example, a progressive change in the number of carbon atoms from 2 to 12 in $Au_{25}(SCn)_{18}$ does not affect the HOMO-LUMO gap, which remains constant at 1.30 eV.[70] Besides these differences, Hg and Cd doping affects the electrochemical potentials very significantly. In particular, the first oxidation of the $Au_{24}M(SC4)_{18}$ clusters occurs ($E°$ values) at -0.188 (Au), +0.364 (Hg), and +0.332 V (Cd).[39] In electrochemical terms, a positive shift of the first oxidation step by more than 0.5 V is indeed massive.

Hg doping induces remarkable changes in the TREPR transients (Figure 7, black trace). First, in $Au_{24}Hg(SC4)_{18}^0$ the photosensitization efficiency is about two thirds that of $Au_{25}(SC4)_{18}^-$ (red trace). This decrease may be caused by a shorter triplet lifetime, a less efficient cluster-to-oxygen energy transfer to form singlet oxygen, or a lower quantum yield for the formation of the triplet. In this context, an important piece of information is provided in a recent study by

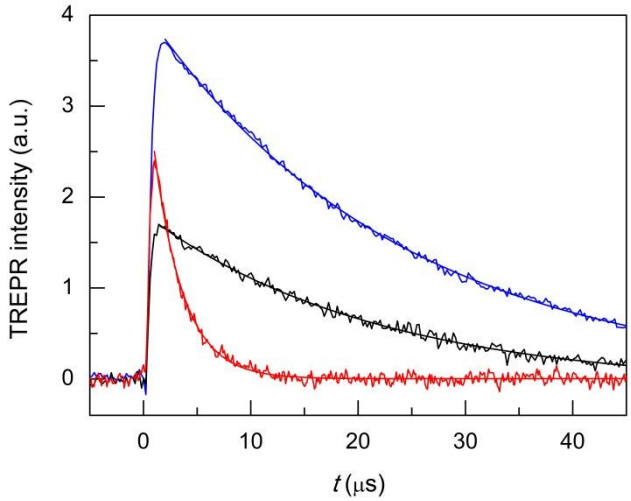


**Figure 7.** Comparison of the TREPR transients and corresponding exponential fit to the data for air-saturated toluene solutions of 0.5 mM TEMPONE and 1 mM $Au_{24}Hg(SC4)_{18}^0$ (black), $Au_{24}Cd(SC4)_{18}^0$ (blue), and $Au_{25}(SC4)_{18}^-$ (red). Temperature = 240 K.

Zhou et al. about the excited-state lifetime of similar (R = C2Ph) clusters, as the values determined for $Au_{24}Hg(SC2Ph)_{18}^0$ and $Au_{25}(SC2Ph)_{18}^-$ are 50 and 100 ns, respectively.[75] The observed TREPR intensities are indeed in rather good agreement with this ratio, and therefore, we may arguably conclude that the efficiency of singlet-oxygen generation is mainly determined by the cluster triplet lifetime. Regarding the hypothesis of a less efficient cluster-to-oxygen energy transfer, we note that the HOMO-LUMO gap of $Au_{24}Hg(SC4)_{18}^0$ (1.28 eV) is slightly smaller than for $Au_{25}(SC2Ph)_{18}^-$ (1.30 eV): the same should be true also for the corresponding triplet states and this may affect the cluster-oxygen energy transfer, although to a very small extent. Finally, ISC in the cluster should occur on the low ns timescale and very efficiently ($\Phi_T$ = 0.87), as evaluated by Wen *et al.* for films of BSA-protected $Au_{25}$ clusters.[76]

The most important effect brought about by the introduction of a single Hg atom, however, is to increase the singlet-oxygen lifetime by more than one order of magnitude: 19.5(0.2) ($k_\Delta = 5.13 \times 10^4$ $s^{-1}$, $r^2 = 0.990$) vs 2.71 μs ($k_\Delta = 3.69 \times 10^5$ $s^{-1}$), which indicates that the mechanism of $^1O_2$ quenching is much less efficient than for the corresponding $Au_{25}$ cluster.

View Article Online
DOI: 10.1039/D0SC00520G



Still, compared with the reference $\tau_\Delta^S$ of 34.6 μs, the relative $\tau_\Delta$ decrease is quite significant: 43.6%.

To make the cluster even more performing, the foreign-metal atom should minimize quenching effects without losing the photosensitization efficiency or possibly even increasing it with respect to $Au_{25}$. The doped cluster should, therefore, exhibit electrochemical properties similar to those of $Au_{24}Hg(SC4)_{18}^0$, a more significant population of the photogenerated triplet state, and ultimately, allow for a longer $^1O_2$ lifetime. A cluster that satisfies these requirements is $Au_{24}Cd(SC4)_{18}^0$, as it is almost as resistant toward oxidation than $Au_{24}Hg(SC4)_{18}^0$ (0.332 V vs 0.364 V), its HOMO-LUMO gap is the largest of the three SC4 clusters, and according to Zhou et al.[75] its excited-state lifetime (in supposedly aerated solution) is 200 ns (R = C2Ph), *i.e.*, two and four times longer than those of $Au_{25}(SC2Ph)_{18}^-$ and $Au_{24}Hg(SC2Ph)_{18}^0$, respectively. In this regard, it is worth mentioning that TREPR (emission decay lifetime of 0.44(0.01) μs, $r^2$ = 0.988) points to a higher limit of ~0.3 μs for the lifetime of the triplet of $Au_{24}Cd(SC4)_{18}^0$ under anaerobic conditions (Figure S4), as already noted and discussed for $Au_{25}(SC3)_{18}^-$. These general expectations of better performance are fully met: use of the Cd-doped cluster yields a longer singlet-oxygen lifetime ($k_\Delta$ = 4.31 × $10^4$ $s^{-1}$, $r^2$ = 0.999, $\tau_\Delta$ = 23.2(0.09) μs) than $Au_{24}Hg(SC4)_{18}^0$, a smaller relative $\tau_\Delta$ decrease (32.9%), and a more significant photosensitization efficiency (Figure 7, blue trace). In particular, the maximum intensity of the TREPR signals is ~1.5 times larger than that observed for $Au_{25}(SC4)_{18}^-$ and more than two times larger than that of $Au_{24}Hg(SC4)_{18}^0$. The photosensitization efficiency of $Au_{24}Cd(SC4)_{18}^0$ is significant also in comparison with the TPP photosensitizer, as the TREPR signal intensity of the former is ~1/2 that of TPP. That the amount of triplet excited state obtained from $Au_{24}Cd(SC4)_{18}^0$ is quite significant is also supported by the presence of the negative spike for $t$ < 0.5 μs, which, as already commented upon for TPP, is attributed to the Q-RTP component (eq 1).

Finally, we tested the Cd-doped cluster that has an even more positive oxidation potential, $Au_{24}Cd(SC2Ph)_{18}^0$, whose $E°$ is 0.430 V (vs 0.332 V for $Au_{24}Cd(SC4)_{18}^0$).[39] The DPV curves (oxidation region) of all clusters investigated and TPP are gathered in Figure 8. Also for this cluster we estimate (Figure S5: TREPR emission decay lifetime of 0.44(0.01) μs, $r^2$ = 0.989) a higher limit of ~0.3 μs for its triplet lifetime under anaerobic conditions. Indeed, the photosensitization outcome further improves (Figure 9, blue trace), as the observed singlet-oxygen lifetime is even longer ($k_\Delta$ = 3.58 × $10^4$ $s^{-1}$, $r^2$ = 0.997, $\tau_\Delta$ = 27.9(0.25) μs). In particular, this $\tau_\Delta$ value and the relative $\tau_\Delta$

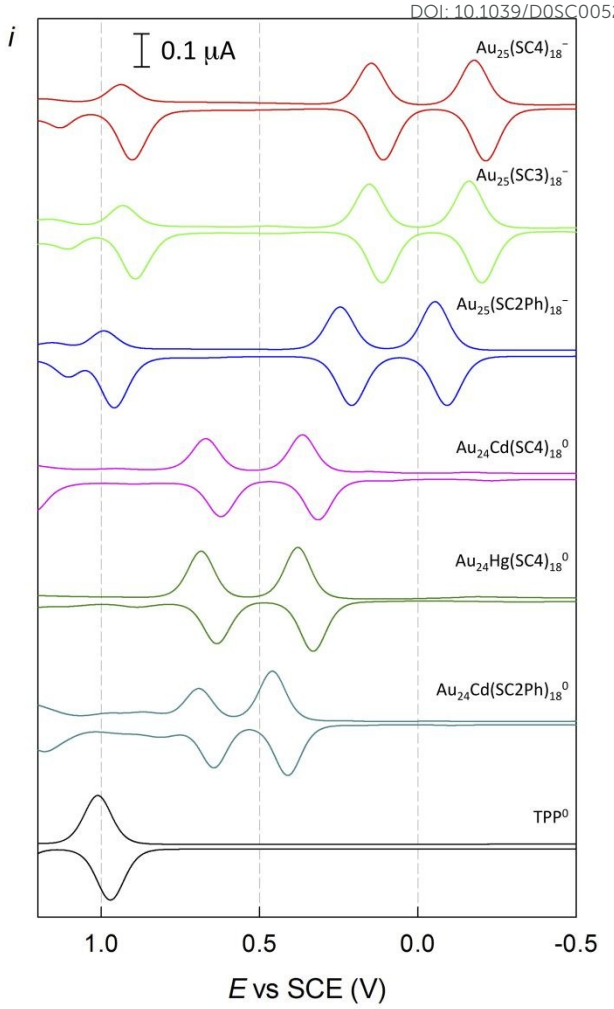


**Figure 8.** Comparison between the DPV curves (oxidation region) of $Au_{25}(SC4)_{18}^-$, $Au_{25}(SC3)_{18}^-$, $Au_{25}(SC2Ph)_{18}^-$, $Au_{24}Cd(SC4)_{18}^0$, $Au_{24}Hg(SC4)_{18}^0$, $Au_{24}Cd(SC2Ph)_{18}^0$, and TPP. Glassy carbon electrode, DCM/0.1 M TBAH, 25 °C.

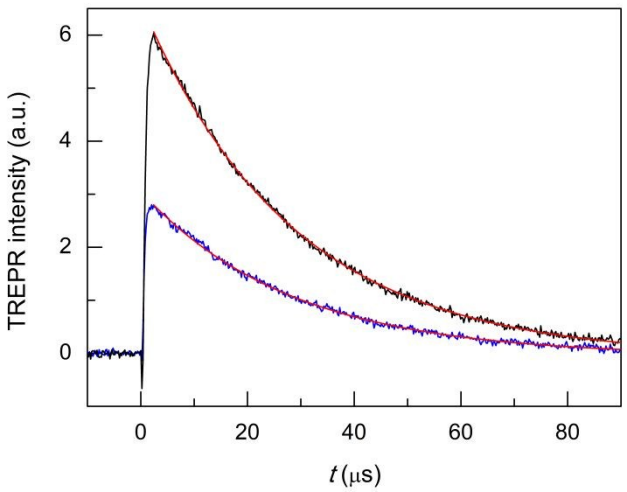


**Figure 9.** TREPR transients and corresponding exponential fit to the data for air-saturated toluene solutions of 0.5 mM TEMPONE and 1 mM $Au_{24}Cd(SC2Ph)_{18}^0$ (blue) and TPP (black). Temperature = 240 K.

decrease, 19.3%, are virtually identical to those of TPP (Figure 9, black trace), 28.2(0.1) μs and 18.5%, though the latter is more difficult to oxidize by as much as 0.563 V (Figure 8). Besides the redox potentials, a comparison between the aforementioned estimated lifetime values (aerobic vs anaerobic conditions) obtained for the Cd-doped clusters and TPP (whose triplet-state lifetime in the absence of oxygen increases by orders of magnitude)[13,62] shows that despite the much shorter intrinsic lifetime of their triplet state, the Cd-doped clusters are perfectly fine to accomplish the $^1O_2$ photosensitization job very efficiently.

**Chemical Quenching**

To compare further the performance of doped and undoped clusters, we performed photosensitization experiments in the presence of 9,10-diphenylanthracene (DPA), which reacts with singlet oxygen to yield the endoperoxide 9,10-diphenyl-9,10-epidioxyanthracene (DPA-$O_2$) with rate constants on the order of $10^6$ $M^{-1}$ $s^{-1}$.[77] Its formation can be conveniently monitored through the decrease in the excitation and fluorescence spectra of DPA. Figure 10 compares the fluorescence spectra of DPA in air-saturated toluene (at room temperature) containing the photosensitizer $Au_{24}Cd(SC4)_{18}^0$ (panel a) or $Au_{25}(SC4)_{18}^-$ (panel b) before and after 10 min pulsed irradiation (carried out as in the TREPR experiments) with a 532 nm laser at 240 K (for details, see Experimental section).

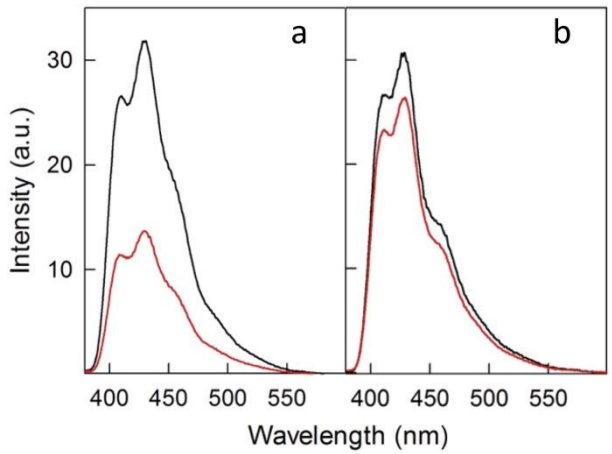


**Figure 10.** Emission spectra ($\lambda_{exc}$ = 360 nm) of 1.3 x $10^{-3}$ mM DPA in aerated toluene containing 0.13 mM (a) $Au_{24}Cd(SC4)_{18}^0$ or (b) $Au_{25}(SC4)_{18}^-$. The spectra correspond to before (black) and after 10 min irradiation (red) at 532 nm at 240 K. The spectra were obtained at room temperature.

For $Au_{24}Cd(SC4)_{18}^0$, the strong emission band of DPA at ~430 nm (excitation at 360 nm) is markedly quenched (by 56.9%), which confirms its particular efficiency as a photosensitizer. Instead, when $Au_{25}(SC4)_{18}^-$ is used as photosensitizer, only 13.6% quenching of the DPA emission is observed at ~430 nm. The different behavior of the two clusters is also quantitatively detected in the excitation spectra obtained at 450 nm: $Au_{24}Cd(SC4)_{18}^0$ causes a strong decrease of the absorption band of DPA (56.9%), whereas the variation is much less significant for $Au_{25}(SC4)_{18}^-$ (11.0%) (Figures S6 and S7). The absorption spectra of the solutions of the two clusters, which only show the optical features of the nanoclusters because their concentration is 100 times larger than that of DPA (the molar extinction coefficients of DPA,[78] $Au_{24}Cd(SC4)_{18}^0$, and $Au_{25}(SC4)_{18}^-$ are 1.4 x $10^4$ $M^{-1}$ $cm^{-1}$ (372.5 nm), 4.68 x $10^4$ $M^{-1}$ cm $^{-1}$ (398 nm) and 4.58 x $10^4$ $M^{-1}$ cm $^{-1}$ (401 nm), respectively), exhibit no differences before and after laser irradiation (Figures S8 and S9), thereby pointing to their photostability (no change of the spectrum associated with cluster oxidation) in the given experimental conditions. These results thus show that $Au_{24}Cd(SC4)_{18}^0$ is a significantly better photosensitizer than $Au_{25}(SC4)_{18}^-$, in full agreement with the TREPR results.

**Mechanism of Physical Quenching by $Au_{25}$ Nanoclusters**

The sequence of the observed $\tau_\Delta$ values is in very good agreement with the cluster oxidation potentials (Figure 11).

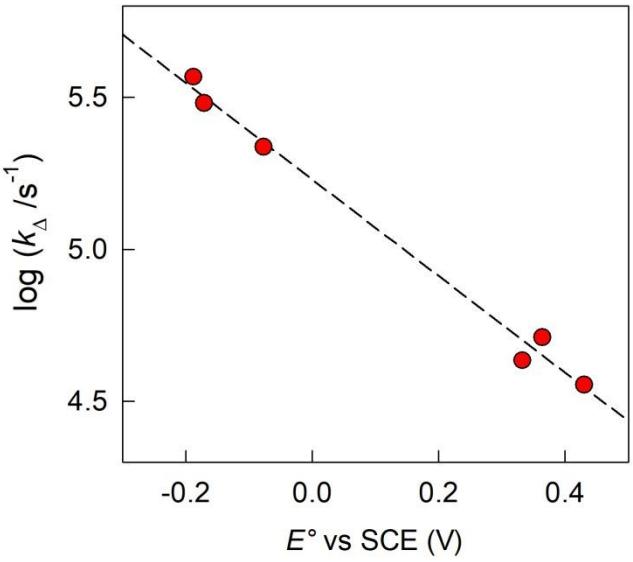


**Figure 11**. Dependence of the $^1O_2$ decay rate constant $k_\Delta$ on the formal potentials for the oxidation of the clusters. The dashed line shows the linear fit to the data.

Due to the aforementioned considerations regarding $k_r$ and $k_{cr}$, eq 5 can be simplified to eq 6:

(6) $k_\Delta = k_{nr}[S] + k_q[M]$

$k_q$ can thus be obtained from the $k_\Delta$ value determined experimentally and the $k_{nr}[S]$ term, which can be calculated from literature data[56] to be 2.89 x $10^4$ $s^{-1}$ at 240 K. According to the CT-ISC mechanism, the quenching process involving $^1O_2$ and the molecular Au nanocluster (M) can be summarized by eqs 7-9:

(7) $$^1O_2 + M \underset{k_{-d}}{\overset{k_d}{\rightleftharpoons}} (^1O_2 , M)$$

(8) $$(^1O_2 , M) \underset{k_{-CT}}{\overset{k_{CT}}{\rightleftharpoons}} {}^1(O_2^{\delta-} , M^{\delta+})$$

(9) $${}^1(O_2^{\delta-} , M^{\delta+}) \xrightarrow{k_{ISC}} {}^3(O_2^{\delta-} , M^{\delta+}) \xrightarrow{k_{-d}} {}^3O_2 + M$$

(10) $$(^1O_2 , M) \underset{k_{-PET}}{\overset{k_{PET}}{\rightleftharpoons}} (O_2^{-\bullet} , M^{+\bullet})$$

(11) $$(O_2^{-\bullet} , M^{+\bullet}) \xrightarrow{k_{-ET}} (^3O_2 , M) \xrightarrow{k_{-d}} {}^3O_2 + M$$

(12) $$(O_2^{-\bullet} , M^{+\bullet}) \xrightarrow{k_{-d}} O_2^{-\bullet} + M^{+\bullet}$$

where, $k_d$ and $k_{-d}$ are the diffusion rate constants for the formation and dissociation of the caged species, $k_{CT}$ and $k_{-CT}$ are the forward and backward rate constants of the transfer of a partial charge $\delta$ between the caged $^1O_2$,M species, and $k_{ISC}$ is the rate constant for ISC in the exciplex. Reactions 10-12 can be competitive to the sequence 8-9 in quenching $^1O_2$: whereas $k_{PET}$ and $k_{-PET}$ are the forward and backward rate constants for the oxidation of the cluster by $^1O_2$ (that is, the possibility of re-crossing to the excited donor surface is included), $k_{-ET}$ is the backward rate constants for the ET between M and $^3O_2$ (that is, charge recombination). It should be noted that eqs 7-12 are generically written for two neutral species. Whereas this is valid for the doped clusters, for $Au_{25}(SR)_{18}^-$ the negative charge of the cluster must be taken into account in eqs 7-12. The fact that the cluster may carry a charge does not prevent the formation of the exciplex, as shown very recently for a cationic excited state acceptor.[79] Charge-transfer activation of oxygen by both anionic and neutral gold nanoclusters has been described.[80,81] Very recent mass spectrometry results would indeed point to an effective interaction of oxygen and $Au_{25}(SC2Ph)_{18}^-$, at least in DCM.[82]

*Charge-transfer Induced Quenching*. We first focus on the quenching sequence 7-9 (the competition by the ET path, eqs 7,10-12, will be discussed later). Applying the steady-state approximation to the encounter complex and the singlet exciplex leads to the following expression (eq 13) for the $k_q$ term in eq. 5:

(13) $$k_q = \frac{k_d}{1 + \frac{k_{-d}}{k_{CT}} + \frac{k_{-d}}{k_{ISC}} exp\left(\frac{\Delta G^\circ_{CT}}{RT}\right)}$$

We start by considering $Au_{25}(SC4)_{18}^-$, which exhibits the less positive oxidation potential and the fastest quenching rate, and then we will discuss the differences caused by making the cluster oxidation more difficult. For this cluster, $k_\Delta$ = 3.69 x $10^5$ $s^{-1}$. The term $k_q$[M] can be obtained from eq 6 by subtracting the rate constant for the intrinsic $^1O_2$ lifetime ($\tau_\Delta^S$ = 34.6 µs, $k_\Delta^S = k_{nr}$[S] = 2.89 x $10^4$ $s^{-1}$). Hence, a value of $k_q$ = 3.40 x $10^8$ $M^{-1}s^{-1}$ is calculated using [M] = 1 mM.

The diffusion rate constants $k_d$ and $k_{-d}$ are estimated to be 1.9 x $10^{10}$ $M^{-1}$ $s^{-1}$ and 2 x $10^{10}$ $s^{-1}$, respectively (see ESI). The equilibrium constant $K_{CT}$, and thus $\Delta G^\circ_{CT}$, is unknown. However, $\Delta G^\circ_{CT}$, which refers to the transfer of the charge fraction $\delta$, is conceivably related to $\Delta G^\circ_{ET}$,[10] which is the free energy for full ET between the cluster and singlet oxygen (eq 10). $k_{CT}$ may be similarly estimated (eq 14) using a Marcus expression for the activation free energy $\Delta G^{\neq}_{CT}$ (eq 15).

(14) $$k_{CT} = Z \exp[-\Delta G^{\neq}_{CT}/RT]$$

(15) $$\Delta G^{\neq}_{CT} = \Delta G_0{}^{\neq}_{CT} [1+ (\Delta G^\circ_{CT}/4\Delta G_0{}^{\neq}_{CT})]^2$$

The process is considered adiabatic and thus occurring at contact distance between singlet oxygen and the cluster, as supported by recent results.[80-82] The frequency factor $Z$ is estimated (see ESI) by taking into account the role of solvent friction in determining the rate of crossing the barrier.[83] $\Delta G_0{}^{\neq}_{CT}$ is the intrinsic barrier, that is, the value of $\Delta G^{\neq}_{CT}$ at zero driving force. In analogy to the ET intrinsic barrier ($\Delta G_0{}^{\neq}_{ET}$), $\Delta G_0{}^{\neq}_{CT}$ can be seen as composed of a solvent reorganization term, $\Delta G_{0,s}{}^{\neq}_{CT}$, and an inner component, $\Delta G_{0,i}{}^{\neq}_{CT}$, which describes the molecular deformation of bond lengths and angles of the reacting system. For a full ET,[84,85] $\Delta G_0{}^{\neq}_{ET}$ can be calculated from the homogeneous self-exchange $(\Delta G_0{}^{\neq}_{ET})_{hom,ex}$ values of the two redox couples (here, $M^{+\bullet}$/M and $^1O_2/O_2^{-\bullet}$) (eq 16):

(16) $$\Delta G_0{}^{\neq}_{ET} = [(\Delta G_0{}^{\neq}_{ET})_{hom,ex,M+\bullet/M} + (\Delta G_0{}^{\neq}_{ET})_{hom,ex,O2/O2-\bullet}]/2$$

The values of the two $(\Delta G_0{}^{\neq}_{ET})_{hom,ex}$ terms can be obtained from the corresponding heterogeneous intrinsic barriers through equation 17:[86]

(17) $$(\Delta G_0{}^{\neq})_{hom,ex} = 2(\Delta G_0{}^{\neq})_{het} - (\Delta G_{0,s}{}^{\neq})_{hom,ex}$$

where $(\Delta G_{0,s}{}^{\neq})_{hom,ex}$ is the homogeneous solvent reorganization term. For the cluster, we use the electrochemical $(\Delta G_0{}^{\neq}_{ET})_{het}$ = 0.222 eV, which was previously obtained in DCM/0.1 M TBAH, at 298 K from the standard heterogeneous rate constant.[69] For $^1O_2/O_2^{-\bullet}$ and assuming that the intrinsic barriers of $^1O_2/O_2^{-\bullet}$ and $^3O_2/O_2^{-\bullet}$ are the same, we obtain $(\Delta G_0{}^{\neq}_{ET})_{het}$ = 0.408 eV by cyclic-voltammetry analysis of the oxygen reduction peak (see Experimental section). To estimate these parameters for toluene at 240 K and then calculate the other terms of eq 17, we followed a procedure described in the ESI. For the $^1O_2/Au_{25}(SC4)_{18}^-$ system, use of eq 16 yields $\Delta G_0{}^{\neq}_{ET}$ = 0.23 eV. It is worth mentioning that for DCM at 298 K, $\Delta G_0{}^{\neq}_{ET}$ is much larger, 0.40 eV: this is a consequence of the fact that the very low polarity of toluene makes the solvent reorganization term very small, with the result that the already significant inner reorganization of $Au_{25}$ clusters[69-71,87] and possibly oxygen[88] becomes largely dominant (85%). For this reason, we can neglect that whereas for $(\Delta G_0{}^{\neq}_{ET})_{het}$ (and thus $(\Delta G_0{}^{\neq})_{hom,ex}$) the radii employed in the solvent reorganization calculations are correct, $(\Delta G_0{}^{\neq})_{ET}$ might be slightly affected by the penetration

of $^1O_2$ inside the monolayer, as the effective cluster radius should be a bit smaller. A posteriori, we checked that this assumption is indeed valid for the CT-ISC mechanism even if one uses for the cluster just the crystallographic radius of the gold core (4.9 Å).[70]

Both $k_{CT}$ and $K_{CT}$ require calculating $\Delta G°_{ET}$ and how to relate it to $\Delta G°_{CT}$. Additionally, $k_{CT}$ requires converting $\Delta G_0^{\neq}{}_{ET}$ into $\Delta G_0^{\neq}{}_{CT}$. For $^1O_2$ quenching, $\Delta G°_{CT}$ is usually taken as a fraction $f$ of $\Delta G°_{ET}$ to account for the partial character $\delta$ of ET in the formation of the exciplex.[10] $\Delta G°_{ET}$ can be estimated, according to Rehm and Weller,[89,90] with eq 18. Because the process here considered involves a neutral and a charged species, $^1O_2/Au_{25}(SC4)_{18}^-$, the Coulombic term associated with formation of charges is zero. To avoid confusion, the actual charge of the $Au_{25}$ cluster is made explicit.

(18) $\Delta G°_{ET} = nFE°(M^{\bullet}/M^-) - nFE°(O_2/O_2^{-\bullet}) - E_{exc}$

where $n$ is the number of exchanged electrons (for a full ET, $n$ = 1), $F$ is the Faraday constant, $E°(M^{\bullet}/M^-)$ and $E°(O_2/O_2^{-\bullet})$ are the formal potentials of the $M^{\bullet}/M^-$ and oxygen/superoxide redox couples, respectively, and $E_{exc}$ = 94 kJ mol$^{-1}$ is the $^3\Sigma_g^-$ to $^1\Delta_g$ excitation energy. Eq 18 (also in its form including the Coulombic term) provides a reasonable estimate of $\Delta G°_{ET}$, and therefore, $E°(^1O_2/O_2^{-\bullet})$ will be taken as $E°(O_2/O_2^{-\bullet}) - E_{exc}/F$ = -0.850 + 0.974 = 0.124 V (for details, see ESI).

As to the fraction $f$ of $\Delta G°_{ET}$, it has been proposed that $\delta \sim f^{1/2}$, as inferred from experimental trends involving neutral donors.[10] Because of the charge here involved, however, we will use a linear dependence (eq 19) in which $\delta$ simply replaces $n$ = 1 in eq 18. Hence:

(19) $\Delta G°_{CT} = \delta F[E°(M^{\bullet}/M^-) - E°(^1O_2/O_2^{-\bullet})]$

Regarding the conversion of $\Delta G_0^{\neq}{}_{ET}$ into $\Delta G_0^{\neq}{}_{CT}$, we consider that $\Delta G_{0,s}^{\neq}{}_{CT}$ should also depend on the square of $\delta$, whereas $\Delta G_{0,i}^{\neq}{}_{CT}$ has been previously considered as, possibly, independent of it, although differences were noted between different classes of compounds.[91] The actual dependence of $\Delta G_0^{\neq}{}_{CT}$ on $\delta$ is indeed unclear, especially in solvent of very low dielectric constant and/or when $\Delta G_{0,i}^{\neq}{}_{CT}$ is dominant, as noted above for $Au_{25}$ clusters.[69-71,87] Here, to balance contributions, we will consider a simple linear dependence, $\Delta G_0^{\neq}{}_{CT} \sim \delta \Delta G_0^{\neq}{}_{ET}$.

$k_{CT}$ can now be obtained from the appropriate preexponential factor (eqs 14 and S1, with $Z$ = 4.6 x 10$^{10}$ s$^{-1}$), provided a reasonable $\delta$ value is used in eq 19. As $\delta$ is unknown, we will follow an approach similar to that used for other series of photosensitizers.[10,66,67] In ETs, the transfer coefficient α is introduced to describe how the activation free energy responds to changes in the reaction driving force, that is, $\alpha = d\Delta G^{\neq}{}_{ET}/d\Delta G°_{ET} = -RTd\ln k_{ET}/d\Delta G°_{ET}$. Because of the quadratic expression relating $\Delta G^{\neq}{}_{ET}$ to $\Delta G°_{ET}$, α is expected to be 0.5 at zero driving force.[85] We will focus on the three $Au_{25}$ clusters, which are self-consistent in terms of cluster charge. The corresponding driving forces for ET (eq 18) range from -0.312 (SC4) to -0.201 (SC2Ph) eV, that is, these processes are exergonic, yet not too far from $\Delta G°_{ET}$ = 0. The corresponding $\log k_q$ vs $\Delta G°_{ET}$ plot provides a slope corresponding to the very small α value of 0.10. Adjusting $\delta$ in eq 19, shows that α = 0.5 is obtained when $\delta$ = 0.2. This figure corresponds to $\Delta G°_{CT}$ values ranging from -0.06 to -0.04 eV. This value of $\delta$ is indeed quite similar to those previously proposed for $^1O_2$ quenching by other photosensitizers.[10,66,67] We also should note that $\delta$ is expected to decrease for more positive reaction free energies.[79] Using $\delta$ = 0.2, the remaining quantities in eq 13 are defined. Hence, an experimental rate constant (SC4) of $k_q$ = 3.40 x 10$^8$ M$^{-1}$ s$^{-1}$, corresponds to $\Delta G°_{CT}$ = -0.062 eV, $k_{CT}$ = 1.8 x 10$^{10}$ s$^{-1}$, and $k_{ISC}$ = 1.8 x 10$^7$ s$^{-1}$. For common photosensitizers, ISC is a fast process, with rate constant values estimated to be ~10$^{10}$ s$^{-1}$.[66] Despite the several inputs and assumptions and the resulting comparatively small $k_{ISC}$ value, this kinetic analysis would suggest that the same CT-ISC mechanism proposed for $^1O_2$ quenching by other photosensitizers is plausible. Different assumptions on the preexponential factor $Z$ do not affect the value of $k_{ISC}$, as already observed.[66]

*Electron-transfer Induced Quenching*. On the other hand, $Au_{25}$ clusters provide unusually[92] negative free energies for ET. This new situation may indeed make the reactions 10-12 competitive to reactions 8,9. As a matter of fact, we already noted that some oxidation of the $Au_{25}(SC4)_{18}^-$ cluster takes place, which points to the occurrence of reaction 12. Although mechanistically useful, however, this reaction only occurs on a long time scale, and therefore, is not kinetically relevant in consuming the charge-separated pair formed in reaction 10. The quantities already estimated, allow us to estimate the likeliness of this competition/alternative path. Thus, assuming that only the ET (indicated as photoinduced ET, PET, to distinguish it from the ET in eq 11) mechanism (eqs 7,10,11) is responsible for $^1O_2$ quenching, the following expression (eq 20) for $k_q$ ensues:

(20)
$$k_q = \frac{k_d}{1 + \frac{k_{-d}}{k_{PET}} + \frac{k_{-d}}{k_{-ET}} exp\left(\frac{\Delta G°_{PET}}{RT}\right)}$$

where the steady-state approximation has been applied to the encounter complex and the charge-separated pair. The resulting relevant rate constants are $k_{PET}$ = 3.9 x 10$^8$ s$^{-1}$, $k_{-ET}$ = 2.0 x 10$^{10}$ s$^{-1}$. Both ETs can be considered as irreversible because the corresponding $k_{-PET}$ and $k_{ET}$ are 1.1 x 10$^2$ and 2.5 x 10$^{-4}$ s$^{-1}$, respectively, and thus escape from the cage is much faster. In other words, the third term in the denominator of eq 20 is orders of magnitude smaller than the first two terms (1 and 51.3, respectively). The process described in eq 11, is thus essentially rate limited by $k_{PET}$ and corresponds to an ET-induced ISC. Because of the many assumptions involved, all these rate-constant values should be considered only as estimates. Nonetheless, we note that the resulting $k_q$ of 3.6 x 10$^8$ s$^{-1}$ is in full agreement with the actual $k_q$ (assuming that only eqs 7 and 10 are kinetically relevant), and this points to the full ET-ISC sequence as the most probable mechanism, although some contribution from the CT-ISC mechanism cannot be excluded. Different assumptions on the



 

preexponential factor, making it larger, would make $k_{PET}$ exceedingly large. If one now considers $Au_{25}(SC2Ph)_{18}^-$, which of the three $Au_{25}$ clusters is the one exhibiting the most positive oxidation potential, the picture does not change much and similar conclusions can be reached.

It is worth making a comment about the spin constrains. For this ET pathway, the singlet-triplet spin transition rate might affect the overall back ET rate in eq 11. Indeed, spin-forbidden transitions can be orders of magnitude slower than the corresponding allowed transition.[93] Both caged species formed in eq 10 are radicals and the exchange interaction between them gives rise to nondegenerate singlet and triplet states (spin-correlated radical pair). In the present case, the singlet state has a higher energy and, as the precursor is a singlet ($^1O_2$), it is initially more populated. Therefore, the back ET rate constant should be considered as an upper limit. However, the rate is still large enough to make $^3O_2$ formation a very rapid step.

*Quenching by the Doped Clusters*. Regarding the doped clusters, the $\Delta G°_{ET}$ in eq 18 (with $E°(M^{+\bullet}/M)$ in place of $E°(M^{\bullet}/M^-)$) requires adding the Coulombic term, as now two opposite charges form. This correction can be performed for CT according to Rhem-Weller,[89,90] who considered this term as negative (stabilization of the opposite charges) (eq 21):

$$(21)\ \Delta G°_{CT} = \delta F[E°(M^{+\bullet}/M) - E°(^1O_2/O_2^{-\bullet})] + (+\delta)(-\delta)\, e^2/4\pi\varepsilon_s\varepsilon_0 a$$

where $e$ is the charge of the electron and $a$ is the distance between the two species (usually taken as the sum of the two radii, assuming the species as spherical). The larger the $\delta$ and the smaller the $\varepsilon_s$, the larger the negative contribution to $\Delta G°_{CT}$. For photoinduced ETs, Coulombic stabilization has been shown to be especially important for dielectric constants smaller than 13.[94]

It is useful to compare TPP and $Au_{24}Cd(SC2Ph)_{18}^0$, which exhibit the very similar $k_q$ values of 6.5 x $10^6$ and 6.9 x $10^6$ $M^{-1}$ $s^{-1}$, respectively. For TPP, the decrease of $\Delta G°_{CT}$ caused by the Coulombic term depends on the value of $\delta$: for example, it is 0.032 and 0.008 eV for $\delta$ = 0.2 and 0.1, respectively. In the absence of further information, however, we will keep using $\delta$ = 0.2. The CT-ISC path can reproduce the experimental $k_q$ value when $k_{ISC}$ is set to 2.4 x $10^{10}$ $s^{-1}$, which is indeed a reasonable value for a molecular system such as TPP.[66] For the sake of arguments, use of the very small $\delta$ value of 0.1 would lower $k_{ISC}$ to 7.5 x $10^8$ $s^{-1}$. Regardless, there is no competition from the ET path (eqs 10,11), as $k_{PET}$ drops by several orders of magnitude.

For $Au_{24}Cd(SC2Ph)_{18}^0$, the situation is more intriguing. Reproducing the observed $k_q$ value, requires $k_{ISC}$ = 3.7 x $10^7$ $s^{-1}$, which, if one considers the error introduced by the various approximations, is probably the same as that calculated for $Au_{25}(SC4)_{18}^-$. On the other hand, the independently estimated $k_{PET}$, 3.2 x $10^6$ $s^{-1}$, leads (eq 20) to $k_q$ = 5.3 x $10^6$ $M^{-1}$ $s^{-1}$, which is also comparable to the experimental value of 6.9 x $10^6$ $M^{-1}$ $s^{-1}$. We are thus facing the same mechanistic competition addressed for the undoped $Au_{25}$ clusters.

## Conclusions

View Article Online
DOI: 10.1039/D0SC00520G

Diamagnetic $Au_{24}M(SR)_{18}$ clusters are shown to be effective singlet-oxygen photosensitizers. As to their efficiency as singlet-oxygen quenchers, we show that it can be modulated quite precisely by changing the ligands and/or one of the Au atoms. Use of the very sensitive TREPR spectroscopy allowed us to determine $^1O_2$ lifetimes ranging from 2.71 to 27.9 µs. The latter, which was measured for $Au_{24}Cd(SC2Ph)_{18}^0$, is virtually the same as that of TPP, a well-known reference photosensitizer.

Analysis of the results leads to three main conclusions.

1. We have described the first kinetic analysis of the quenching mechanism/s by gold nanoclusters. The $Au_{25}$ clusters have unusually low $E°$ values, yielding almost unprecedented[92] negative $\Delta G°_{ET}$ values. $^1O_2$ quenching involves both CT-ISC and ET-ISC mechanisms, although the latter appears to be the most probable: indeed, whereas for the ET-ISC mechanism the $k_q$ value is fully calculated according to eq 20, for the CT-ISC mechanism the $k_{ISC}$ is adjusted to reproduce the experimental $k_q$ value via eq 13. Therefore, the actual $k_{ISC}$ might be even smaller. This is also supported by the fact that $^1O_2$ quenching by the corresponding $Au_{24}M$ doped clusters also appears to be possible through both mechanisms. The ET-ISC mechanism is made possible because the substantially more positive $E°$s of these doped clusters are largely compensated by the Coulombic term (eq 21). This would imply that the use of a more polar solvent, which decreases the value of the Coulombic term[89,90] and may even revert its sign,[94] would remove the feasibility of the ET-ISC mechanism, leaving the CT-ISC as the only plausible quenching mechanism.

2. Despite the possibility of quenching $^1O_2$ through two mechanisms, we have detected the striking effect that the $k_{ISC}$ values estimated for the nanoclusters are consistently smaller than those estimated for other molecular systems (and here shown for TPP) by *no less than two orders of magnitude*. This observation is obviously beneficial in terms of using this family of nanoclusters as $^1O_2$ photosensitizers with minimum $^1O_2$ quenching efficacy, and makes these materials extremely promising for practical applications. Indeed, this large difference in $k_{ISC}$ values points to something special in the interaction between nanoclusters and $^1O_2$. Minaev concluded that, to achieve an efficient intersystem crossing enhancement, there should be a non-linear encounter geometry between $^1O_2$ and the quencher molecular axes.[68,93] This condition is typically fulfilled for common molecules, as quenching can be treated as a series of random encounters. Instead, ligand-protected gold nanoclusters are composed of a hard core and a dynamic capping layer,[69] which is a feature not present in regular molecules. When inside the monolayer, interactions of $^1O_2$ with the ligands may give rise to orientation-specific interactions with the Au orbitals. In this framework, our results would suggest that an approximately axial collision takes place, as this orientation, according to Minaev, does not lead to strong ISC. More generally, it is conceivable that the limited orientations imposed by the

View Article Online
DOI: 10.1039/D0SC00530G



capping monolayer can make ISC substantially less favored than in common molecular systems, where all relative orientation geometries and, therefore, ISC contributions are possible.

3. The sequence of the observed $\tau_\Delta$ values illustrated in Figure 11 demonstrates that the efficiency of $Au_{24}M(SR)_{18}$ clusters as singlet oxygen quencher is a function of their $E°$ value. We thus expect that a more positive $E°$ would allow us to obtain even better results, and possibly reach the physiological limit of $\tau_\Delta^S$ = 34.6 μs, i.e., no physical quenching by the cluster. According to Figure 11, whose linear fit has the good $r^2$ value of 0.990, the "ideal" cluster should have an oxidation potential at least more positive than ~0.5 V vs SCE in DCM/0.1 M TBAH. We believe that this target is indeed reachable through proper selection of the ligands to cap a cluster of the $Au_{24}Cd(SR)_{18}^0$ family, which also appears to have the longest triplet lifetime.

These results, methodologies, insights, and conclusions are expected to provide further ideas and incentive for using atomically precise gold nanoclusters as efficient photosensitizers, which is a topic of current interest for both fundamental and applied research.[95,96]

## Experimental

**TREPR**

For the TREPR measurements, a pulsed laser beam from a Nd:YAG laser (Quantel Brilliant, pulse length 5 ns, pulse energy 5 mJ, pulse repetition rate 20 Hz) was used for the optical excitation of the samples at 532 nm. At this wavelength, the absorption of all $Au_{24}M(SR)_{18}$ clusters is significantly larger than for nitroxides. The measurements were carried out by using a Bruker ER200D (X-band) spectrometer with an extended detection bandwidth (6 MHz), disabling the magnetic field modulation, and working in a direct detection mode. The temperature of the sample inside the EPR cylindrical cavity (8 mm optical access) was controlled to 240 K by a variable-temperature nitrogen flow system. The time-dependent EPR signals were digitized using a digital oscilloscope (LeCroy Model LT344) with a maximum acquisition rate of 500 megasample/s synchronized with the laser pulse. The time resolution of the instrument was ~150 ns. Data collection was performed with a personal computer and software that allowed controlling the magnetic field and setting the digital oscilloscope. Typically, 300 transient signals were averaged at on-resonance conditions and subtracted from those accumulated off-resonance to eliminate the background signal induced by the laser pulse. A complete two-dimensional data set that shows the EPR signal as a function of both time and magnetic field consists typically of a set of transient signals, containing 500 points each, recorded at 128 different magnetic field positions. The 500 × 128 matrix gave a two-dimensional time/field data set from which the transient spectra were extracted.

**Electrochemistry**

The DPV and CV measurements were carried out in DCM/ 0.1 M TBAH, under an Ar atmosphere, in a glass cell, at 25 °C. For DPV we used a CHI 660c electrochemical workstation, whereas for the electrode kinetics CV experiments we used an EG&G-PARC 173/179 potentiostat-digital coulometer, an EG&G-PARC 175 universal programmer, and a Nicolet 3091 12-bit resolution digital oscilloscope. The working electrode was a glassy carbon microdisk ($9.1 \times 10^{-4}$ $cm^2$), prepared and activated as already described.[97] The counter-electrode was a Pt wire. A silver wire, which was kept in a tube filled with the same electrolyte solution and separated from the main compartment by a Vycor frit, served as a quasi-reference electrode. At the end of the experiments, its potential was calibrated after addition of ferrocene; the ferricenium/ferrocene redox couple has $E°$ = 0.460 V (SCE) in DCM/0.1 M TBAH. All potential values are reported against SCE. Standard DPV parameters were employed: peak amplitude = 50 mV, pulse width = 0.05 s, increments per cycle = 2 mV, pulse period = 0.1 s. For CV, we applied the positive feedback correction to minimize the ohmic drop between the working and the reference electrodes. The standard heterogeneous rate constant, $k°_{het}$, for oxygen reduction on a glassy carbon electrode was determined by analysis of the CVs obtained at various scan rates ($v$). In DCM/TBAH 0.1 M, the separation between the cathodic and anodic peak potentials is large also at low $v$ values (*e.g.*, 0.228 V at 0.2 V $s^{-1}$) pointing to a small $k°_{het}$ value. The latter was determined by digital simulation of the experimental CVs. For digital simulation, we used the DigiSim 3.03 software, using a step size of 1 mV and an exponential expansion factor of 0.5.

## Conflicts of interest

There are no conflicts to declare.

## Acknowledgements

This work was financially supported by the University of Padova (P-DiSC-2018: Magnetic detection of singlet oxygen photosensitized by gold nanoclusters; P-DiSC-2017: Gold Nose) and Fondazione CARIPARO (grant: GoldCat).

## Author Contributions

M.A. carried out most of the TREPR measurements and analyses; W.F. prepared and characterized all clusters; S.A. carried out the electrochemical experiments; M.A., T.D. and S.B. conducted the chemical quenching experiments; A.Z. and M.R. contributed to the TREPR study; S.A. and F.M. carried out the kinetic analysis; M.R. and F.M. designed the research; M.A., S.A., M.R., and F.M. wrote the paper.

## References

1 K. H. Becker, W. Groth and U. Schurath, *Chem. Phys. Lett.*, 1971, **8**, 259-262.

2 (a) F. Wilkinson, W. P. Helman and A. B. Ross, *J. Phys. Chem. Ref. Data*, 1995, **24**, 663−1021. (b) F. Wilkinson and J. G. Brummer, *J. Phys. Chem. Ref. Data*, 1981, **10**, 809-999.
3 M. Ruzzi, E. Sartori, A. Moscatelli, I. V. Khudyakov and N. J. Turro, *J. Phys. Chem. A*, 2013, **117**, 5232-5240.
4 I. Amato, *Science*, 1993, **262**, 32-33.
5 A. Greer, *Acc. Chem. Res*., 2006, **39**, 797−804.
6 N. J. Turro, V. Ramamurthy and J. C. Scaiano, *Molecular Oxygen and Organic Photochemistry*, in *Modern Molecular Photochemistry of Organic Molecules*, University Science Books, Sausalito, 2010, Ch. 14, pp. 1001-1042.
7 A. A. Ghogare and A. Greer, *Chem. Rev.*, 2016, **116**, 9994−10034.
8 Y. Nosaka and A. Y. Nosaka, *Chem. Rev.*, 2017, **117**, 11302−11336.
9 D. E. Dolmans, D. Fukumura and R. K. Jain, *Nat. Rev*. *Cancer*, 2003, **3**, 380–387.
10 C. Schweitzer and R. Schmidt, *Chem. Rev.*, 2003, **103**, 1685-1757.
11 P. R. Ogilby, *Chem. Soc. Rev.*, 2010, **39**, 3181-3209.
12 M. Bregnhøj, M. Westberg, B. F. Minaev and P. R. Ogilby, *Acc. Chem. Res.*, 2017, **50**, 1920-1927.
13 M. C. DeRosa and R. J. Crutchley, *Coord. Chem. Rev*., 2002, **233–234**, 351-371.
14 J. R. Hurst, J. D. McDonald and G. B. Schuster, *J. Am. Chem. Soc.*, 1982, **104**, 2065–2067.
15 P. R. Ogilby and C. S. Foote, *J. Am. Chem. Soc.*, 1983, **105**, 3423–3430.
16 A. A. Krasnovsky, Jr., M. E. Bashtanov, N. N. Drozdova, O. A. Yuzhakova and E. A. Luk'yanets, *Quantum. Electron*, 2002, **32**, 83-86.
17 Y. You, *Org. Biomol. Chem.*, 2018, **16**, 4044-4060.
18 R. Jin, C. Zeng, M. Zhou and Y. Chen, *Chem. Rev.*, 2016, **116**, 10346-10413.
19 H. Kawasaki, S. Kumar, G. Li, C. Zeng, D. R. Kauffman, J. Yoshimoto, Y. Iwasaki and R. Jin, *Chem. Mater.*, 2014, **26**, 2777-2788.
20 M. Sakamoto, T. Tachikawa, M. Fujitsuka and T. Majima, *Langmuir*, 2009, **25**, 13888-13893.
21 T. Das, P. Ghosh, M. S. Shanavas, A. Maity, S. Mondal and P. Purkayastha, *Nanoscale*, 2012, **4**, 6018-6024.
22 J. Y. Zhao, R. Cui, Z. L. Zhang, M. Zhang, Z. X. Xie and D. W. Pang, *Nanoscale*, 2014, **6**, 13126-13134.
23 R. Vankayala, C. L. Kuo, K. Nuthalapati, C. S. Chiang and K. C. Hwang, *Adv. Funct. Mater.*, 2015, **25**, 5934-5945.
24 D. Yang, G. Yang, S. Gai, F. He, G. An, Y. Dai, R. Lv and P. Yang, *Nanoscale*, 2015, **7**, 19568-19578.
25 M. Yamamoto, I. Osaka, K. Yamashita, H. Hasegawa, R. Arakawa and H. Kawasaki, *J. Lumin.* 2016, **180**, 315-320.
26 M. Yamamoto, K. Shitomi, S. Miyata, H. Miyaji, H. Aota and H. Kawasaki, *J. Colloid. Interface Sci.*, 2018, **510**, 221-227.
27 S. Miyata, H. Miyaji, H. Kawasaki, M. Yamamoto, E. Nishida, H. Takita, T. Akasaka, N. Ushijima, T. Iwanaga and Sugaya, *Int. J. Nanomed.*, 2017, **12**, 2703−2716.
28 D. Hikosou, S. Saita, S. Miyata, H. Miyaji, T. Furuike, H. Tamura and H. Kawasaki, *J. Phys. Chem. C*, 2018, **122**, 12494−12501.
29 R. Ho-Wu, S. H. Yau and T. Goodson III, *J. Phys. Chem. B*, 2017, **121**, 10073-10080.
30 G. Zhang, R. Wang and G. Li, *Chin. Chem. Lett.*, 2018, **29**, 687–693.
31 J. Zhang, Z. Li, J. Huang, C. Liu, F. Hong, K. Zheng and G. Li, *Nanoscale*, 2017, **9**, 16879-16886.
32 Z. Li, C. Liu, H. Abroshan, D. R. Kauffman and G. Li, *ACS Catal.*, 2017, **7**, 3368−3374.
33 K. Kawamura, D. Hikosou, A. Inui, K. Yamamoto, J. Yagi, S. Saita and H. Kawasaki, *J. Phys. Chem. C*, 2019, **123**, 26644-26652.
34 S. Antonello and F. Maran, *Curr. Opin. Electrochem*., 2017, **2**, 18−25.
35 a) M. Agrachev, S. Antonello, T. Dainese, M. Ruzzi, A. Zoleo, E. Aprà, N. Govind, A. Fortunelli, L. Sementa and F. Maran, *ACS Omega*, 2017, **2**, 2607-2617; b) Correction to Magnetic Ordering in Gold Nanoclusters, *ACS Omega*, 2017, **2**, 3595.
36 M. Agrachev, M. Ruzzi, A. Venzo and F. Maran, *Acc. Chem. Res*., 2019, **52**, 44−52.
37 J. F. Parker, C. A. Fields-Zinna and R. W. Murray, *Acc. Chem. Res.*, 2010, **43**, 1289−1296.
38 X. Kang, H. Chong and M. Zhu, M. *Nanoscale*, 2018, **10**, 10758-10834.
39 W. Fei, S. Antonello, T. Dainese, A. Dolmella, M. Lahtinen, K. Rissanen, A. Venzo and F. Maran, *J. Am. Chem. Soc.*, 2019, **141**, 16033-16045.
40 A. Kawai, M. Mitsui, Y. Kobori and K. Obi, *Appl. Magn. Reson.*, 1997, **12**, 405-410.
41 C. G. Martinez, S. Jockusch, M. Ruzzi, E. Sartori, A. Moscatelli, N. J. Turro and A. L. Buchachenko, *J. Phys. Chem. A*, 2005, **109**, 10216-10221.
42 C. Corvaja, in *Fullerenes: From Synthesis to Optoelectronic Properties*. Guldi, D. M. and Martin N. Eds., Kluwer Academic Publishers, 2002, pp. 213-236.
43 C. Blättler, F. Jent and H. A. Paul, *Chem. Phys. Lett.*, 1990, **166**, 375-380.
44 K. M. Salikhov, Yu. N. Molin, R. Z. Sagdeev and A. L. Buchachenko, *Spin Polarization and Magnetic Effects in Radical Reactions*, Elsevier, Amsterdam, 1984.
45 M. Mitsui, K. Takeda, Y. Kobori, A. Kawai and K. Obi, *Chem Phys. Lett.*, 1996, **262**, 125-130.
46 M. Mitsui, K. Takeda, Y. Kobori, A. Kawai and K. Obi, *J. Phys. Chem. A*, 2004, **108**, 1120-1126.
47 A. Kawai, T. Okutsu and K. Obi, *J. Phys. Chem.*, 1991, **95**, 9130-9134.
48 M. De Nardi, S. Antonello, D. Jiang, F. Pan, K. Rissanen, M. Ruzzi, A. Venzo, A. Zoleo and F. Maran, *ACS Nano*, 2014, **8**, 8505-8512.
49 M. Agrachev, S. Antonello, T. Dainese, J. A. Gascón, F. Pan, K. Rissanen, M. Ruzzi, A. Venzo, A. Zoleo and F. Maran, *Chem. Sci.*, 2016, **7**, 6910-6918.
50 S. Antonello, T. Dainese, F. Pan, K. Rissanen and F. Maran, *J. Am. Chem. Soc.*, 2017, **139**, 4168–4174.
51 A. Venzo, S. Antonello, J. A. Gascón, I. Guryanov, R. D. Leapman, N. V. Perera, A. Sousa, M. Zamuner, A. Zanella and F. Maran, *Anal. Chem.*, 2011, **83**, 6355–6362.
52 S. Antonello, M. Hesari, F. Polo and F. Maran, *Nanoscale*, 2012, **4**, 5333–5342.
53 I. Rosenthal, *Chemical and Physical Sources of Singlet Oxygen*, in *Singlet $O_2$*, Frimer, A. A., Ed., CRC Press, Boca Raton, 1985, vol. I, pp. 13-38.
54 A. Kawai and K. Shibuya, *J. Photochem. Photobiol. C: Photochem. Rev.*, 2006, **7**, 89–103.
55 M. J. Povich, *J. Phys. Chem.*, 1975, **79**, 1106-1109.
56 M. Bregnhøj, M. Westberg, F. Jensen and P. R. Ogilby, *Phys. Chem. Chem. Phys.*, 2016, **18**, 22946-22961.
57 A. A. Gorman, I. Hamblett, C. Lambert, B. Spencer and M. C. Standen, *J. Am. Chem. Soc*., 1988, **110**, 8053-8059.
58 J. Zhang, C. Jiang, J. P. Figueiró Longo, R. B. Azevedo, H. Zhang and L. A. Muehlmann, *Acta Pharm. Sinica B*, 2018, **8**,137-146.
59 C. Tanielian and C. Wolff, *Photochem. Photobiol*., 1988, **48**, 277-280.
60 S. M. Bachilo and R. B. Weisman, *J. Phys. Chem. A*, 2000, **104**, 7711−7714.
61 C. Tanielian and C. Wolff, *J. Phys. Chem.*, 1995, **99**, 9825-9830.
62 M. Pineiro, A. L. Carvalho, M. M. Pereira, A. M. d'A. Rocha

Gonsalves, L. G. Arnaut and S. J. Formosinho, *Chem. Eur. J.*, 1998, **4**, 2299-2307.
63 C. Ouannès and T. Wilson, *J. Am. Chem. Soc.*, 1968, **90**, 6527-6528.
64 C. Schweitzer, Z. Mehrdad, F. Shafii and R. Schmidt, *Phys. Chem. Chem. Phys*., 2001, **3**, 3095-3101.
65 E. A. Ogryzlo and C. W. Tang, *J. Am. Chem. Soc.*, 1970, **92**, 5034-5036.
66 A. P. Darmanyan, W. S. Jenks and P. Jardon, *J. Phys. Chem. A* 1998, **102**, 7420–7426.
67 C. Schweitzer, Z. Mehrdad, F. Shafii and R. Schmidt, *J. Phys. Chem. A*, 2001, **105**, 5310-5316.
68 B. F. Minaev, *Theor. Exp. Chem*., 1984, **20**, 199−201.
69 S. Antonello, G. Arrigoni, T. Dainese, M. De Nardi, G. Parisio, L. Perotti, A. René, A. Venzo and F. Maran, *ACS Nano*, 2014, **8**, 2788–2795.
70 S. Antonello, T. Dainese, M. De Nardi, L. Perotti and F. Maran, *ChemElectroChem.*, 2016, **3**, 1237–1244.
71 S. Antonello, A. H. Holm, E. Instuli and F. Maran, *J. Am. Chem. Soc.*, 2007, **129**, 9836−9837.
72 S. Wang, Y. Song, S. Jin, X. Liu, J. Zhang, Y. Pei, X. Meng, M. Chen, P. Li and M. Zhu, *J. Am. Chem. Soc.*, 2015, **137**, 4018−4021.
73 C. Yao, Y.-j. Lin, J. Yuan, L. Liao, M. Zhu, L.-h. Weng, J. Yang and Z. Wu, *J. Am. Chem. Soc*., 2015, **137**, 15350−15353.
74 L. Liao, S. Zhou, Y. Dai, L. Liu, C. Yao, C. Fu, J. Yang and Z. Wu, *J. Am. Chem. Soc*., 2015, **137**, 9511−9514.
75 M. Zhou, C. Yao, M. Y. Sfeir, T. Higaki, Z. Wu and R. Jin, *J. Phys. Chem. C*, 2018, **122**, 13435−13442.
76 X. Wen, P. Yu, Y. R. Toh, A. C. Hsu, Y. C. Lee and J. Tang, *J. Phys. Chem. C*, 2012, **116**, 19032-19038.
77 R. Castro-Olivares, G. Günter, A. L. Zanocco and E. Lemp, *J. Photochem. Photobiol. A – Chemistry*, 2009, **207**, 160-166.
78 I. B. Berlman, *Handbook of Fluorescence Spectra of Aromatic Molecules*, Academic Press, New York, 1971.
79 J. P. Dinnocenzo, P. B. Merkel and S. Farid, *J. Phys. Chem. A*, 2017, **121**, 7903−7909.
80 A. P. Woodham, G. Meijer and A. Fielicke, *Angew. Chem., Int. Ed*., 2012, **51**, 4444-4447.
81 A. P. Woodham, G. Meijer and A. Fielicke, *J. Am. Chem. Soc.*, 2013, **135**, 1727-1730.
82 S. Bhat, R. P. Narayanan, A. Baksi, P. Chakraborty, G. Paramasivam, R. R. J. Methikkalam and A. Nag, *J. Phys. Chem. C*, 2018, **122**, 19455-19462.
83 L. D. Zusman, *Chem. Phys*., 1980, **49**, 295-304.
84 N. Sutin, *Progr. Inorg. Chem*, 1983, **30**, 441-498.
85 R. A. Marcus and N. Sutin, *Biochim. Biophys. Acta*, 1985, **811**, 265-322.
86 A. B. Meneses, S. Antonello, M.-C. Arévalo, C. C. González, J. Sharma, A. N. Wallette, M. S. Workentin and F. Maran, *Chem. Eur. J*. **2007**, *13*, 7983-7995.
87 S. Antonello, N. V. Perera, M. Ruzzi, J. A. Gascón and F. Maran, *J. Am. Chem. Soc*., 2013, **135**, 15585–1559.
88 A. Ignaczak, W. Schmickler and S. Bartenschlager, *J. Electroanal. Chem.*, 2006, **586**, 297–307.
89 D. Rehm and A. Weller, *Isr. J. Chem*., 1970, **8**, 259-271.
90 IUPAC. Compendium of Chemical Terminology, 2nd ed. (the "Gold Book"). Compiled by A. D. McNaught and A. Wilkinson. Blackwell Scientific Publications, Oxford (1997). Online version (2019-) created by S. J. Chalk. ISBN 0-9678550-9-8. https://doi.org/10.1351/goldbook.
91 C. Schweitzer, Z. Mehrdad, F. Shafii and R. Schmidt, *Phys. Chem. Chem. Phys*., 2001, **3**, 3095-3101.
92 S. Fukuzumi, S. Fujita, T. Suenobu, H. Yamada, H. Imahori, Y. Araki and O. Ito, *J. Phys. Chem. A*, 2002, **106**, 1241-1247.
93 B. F. Minaev, *Russ. Chem. Rev.*, 2007, **76**, 988-1010.
94 S. Farid, J. P. Dinnocenzo, P. B. Merkel, R. H. Young and D. Shukla, *J. Am. Chem. Soc*., 2011, **133**, 4791−4801.
95 O. J. H. Chai, Z. Liu, T. Chen and J. Xie, *Nanoscale*, 2019, **11**, 20437-20448.
96 T. Kawawaki, Y. Negishi and H. Kawasaki, *Nanoscale Adv.*, 2020, **2**, 17-36.
97 A. B. Meneses, S. Antonello, M.-C Arévalo and F. Maran, *Electroanal.*, 2006, **18**, 363−370.

View Article Online
DOI: 10.1039/D0SC00520G





## Graphical Abstract Text

Atomically precise $Au_{24}M(SR)_{18}$ clusters were used as singlet-oxygen photosensitizers. Comprehensive kinetic analysis provided insights into the mechanism and driving-force dependence of the quenching of $^1O_2$ by gold nanoclusters.

## Graphical Abstract